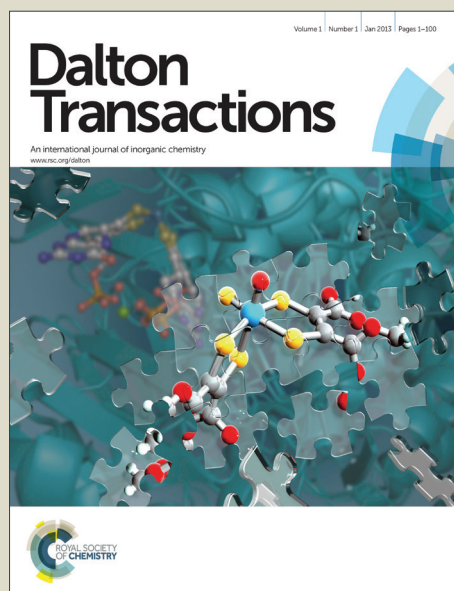


# Dalton Transactions

Accepted Manuscript



This article can be cited before page numbers have been issued, to do this please use: A. R. Chakravarty, S. Banerjee, I. Pant, I. Khan, P. Prasad, A. Hussain and P. Kondaiah, *Dalton Trans.*, 2015, DOI:



This is an *Accepted Manuscript*, which has been through the Royal Society of Chemistry peer review process and has been accepted for publication.

*Accepted Manuscripts* are published online shortly after acceptance, before technical editing, formatting and proof reading. Using this free service, authors can make their results available to the community, in citable form, before we publish the edited article. We will replace this *Accepted Manuscript* with the edited and formatted *Advance Article* as soon as it is available.

You can find more information about *Accepted Manuscripts* in the [Information for Authors](#).

Please note that technical editing may introduce minor changes to the text and/or graphics, which may alter content. The journal's standard [Terms & Conditions](#) and the [Ethical guidelines](#) still apply. In no event shall the Royal Society of Chemistry be held responsible for any errors or omissions in this *Accepted Manuscript* or any consequences arising from the use of any information it contains.

Cite this: DOI: 10.1039/C4DT02165G

www.rsc.org/xxxxxx

ARTICLE TYPE

# Remarkable enhancement in photocytotoxicity and hydrolytic stability of curcumin on binding to an oxovanadium(IV) moiety†

Samya Banerjee,<sup>a</sup> Ila Pant,<sup>b</sup> Imran Khan,<sup>b</sup> Puja Prasad,<sup>a</sup> Akhtar Hussain,<sup>a</sup> Paturu Kondaiah<sup>\*b</sup> and Akhil R. Chakravarty<sup>\*a</sup>

Received (in XXX, XXX) Xth XXXXXXXXX 20XX, Accepted Xth XXXXXXXXX 20XX

DOI: 10.1039/b000000x

Oxovanadium(IV) complexes of polypyridyl and curcumin-based ligands, viz. [VO(cur)(L)Cl] (**1**, **2**) and [VO(scur)(L)Cl] (**3**, **4**), where L is 1,10-phenanthroline (phen in **1** and **3**), dipyrido[3,2-a:2',3'-c]phenazine (dppz in **2** and **4**), Hcur is curcumin and Hscur is diglucosylcurcumin, were synthesized, characterized and their cellular uptake, photocytotoxicity, intracellular localization, DNA binding, DNA photo-cleavage activity studied. Complex [VO(cur)(phen)Cl] (**1**) has V<sup>IV</sup>N<sub>2</sub>O<sub>3</sub>Cl distorted octahedral geometry as evidenced from its crystal structure. The sugar appended complexes show significantly higher uptake into the cancer cells compared to their normal analogues. The complexes are remarkably photocytotoxic in visible light (400-700 nm) giving an IC<sub>50</sub> value of <5 μM in HeLa, HaCaT and MCF-7 cells with no significant dark toxicity. The green emission of the complexes was used for cellular imaging. Predominant cytosolic localization of the complexes **1-4** with a lesser extent into the nucleus was evidenced from confocal imaging. The complexes as avid binders to calf thymus DNA displayed photocleavage of supercoiled pUC19 DNA in red light by generating •OH radicals as the ROS. The cell death is via apoptotic pathway involving the ROS. Binding to the VO<sup>2+</sup> moiety has resulted stability against any hydrolytic degradation of curcumin along with an enhancement of its photocytotoxicity.

## Introduction

Photodynamic therapy (PDT) has emerged as a new modality for the selective treatment of various types of cancers by killing the photo-exposed cancer cells without harming the unexposed healthy cells. The FDA approved PDT drug Photofrin<sup>®</sup> is a hematoporphyrin derivative that requires light and oxygen to initiate photochemical reaction that leads to generation of highly reactive singlet oxygen (<sup>1</sup>O<sub>2</sub>) which causes death of the cancer cells.<sup>1-3</sup> Other macrocyclic organic dyes are also known for their PDT activity. Such dyes generally show severe side effects like skin photo-sensitivity and hepatotoxicity due to oxidative degradation of the macrocyclic core.<sup>4,5</sup> These predicaments could be surmounted by designing transition metal complexes having bio-compatible photosensitizers like curcumin and related dyes that are active in the PDT spectral window. Different types of metal-based photocytotoxic agents are now reported to show significant PDT activity.<sup>6-10</sup> Transition metal complexes with

50

their tunable coordination geometry are suitable for ligating the metal to various chromophores having pendant tumor targeting moieties for their photo-activity and enhanced uptake into the cancer cells for reduced side-effects to normal cells. The versatile redox properties of such complexes could provide an alternative pathway, viz. photo-redox pathway to be operative for the generation of different radical species, viz. •OH and superoxide radical. The photophysical properties of the complexes with low energy d-d or charge-transfer (CT) band are of importance as the complexes could be activated by visible or preferably near-IR red light making such complexes as the promising alternatives to Photofrin<sup>®</sup>.

We have shown in a recent communication that curcumin (Hcur) which is well known for its remarkable medicinal properties could be successfully used as a novel photosensitizer-cum-cellular imaging agent when bound to an oxovanadium(IV) moiety.<sup>11</sup> Curcumin, 1,7-bis-(4-hydroxy-3-methoxyphenyl)-1,6-heptadiene-3,5-dione, is used as traditional herbal medicine to treat infections, bite, burns and skin diseases besides a wide range of other biological activities.<sup>12</sup> Curcumin as an anticancer drug stops tumor progression by inhibiting angiogenesis in cultured endothelium vascular cells and animal model.<sup>13</sup> Studies with *in vitro* models have revealed that it induces apoptosis via mitochondrial pathways involving caspases and Bcl-2 family of proteins.<sup>14,15</sup> It also interferes with the activity of the transcription

<sup>a</sup> Department of Inorganic and Physical Chemistry, Indian Institute of Science, Bangalore 560012, India. Fax: +91-80-23600683; Tel: +91-80-22932533; E-mail: arc@ipc.iisc.ernet.in

<sup>b</sup> Department of Molecular Reproduction, Development and Genetics, Indian Institute of Science, Bangalore 560012, India.

<sup>†</sup> Electronic Supplementary Information (ESI) available: ESI-MS and IR spectra, cyclic voltammograms, energy minimized structures, cellular data, DNA binding and cleavage data (Fig. S1-S36). For ESI or other electronic format See DOI: 10.1039/b000000x/

factor NF- $\kappa$ B which is known to enhance the activity of the tumor suppressor protein p53.<sup>16,17</sup> In addition, curcumin with cisplatin is reported to enhance the reduction of head and neck cancer cell growth.<sup>18</sup> With all these positive aspects, clinical application of curcumin (Hcur) as such is severely limited due to its poor bioavailability, pharmacokinetic profile resulting from its hydrolytic instability under physiological conditions, associated skin sensitivity and intestinal disorders when taken in its native form in higher dose. The hydrolytic instability is due to the presence of a highly reactive  $\beta$ -diketone moiety.<sup>19</sup> Microscopic imaging studies with curcumin alone show complete disappearance of its fluorescence intensity during the cellular incubation period.<sup>11</sup> Binding of this  $\beta$ -diketone moiety in its enolic form to an oxophilic metal centre increases the stability of curcumin and the resulting complexes show remarkable cytotoxic or photocytotoxic activity.<sup>11,20-23</sup> The metal-based curcumin complexes are thus emerging as a new class of non-porphyrinic PDT agents. The monoanionic curcumin ligand as a photosensitizer with a visible band near 440 nm and as a fluorophore with green emission property is suitable for dual applications, viz. (i) imaging the cells by fluorescence microscopy to study cellular localization of the complexes and (ii) damaging the cells on irradiation with a visible light (400-700 nm).

The present work stems from our interest to increase the bioavailability of curcumin on complexation with a VO<sup>+2</sup> moiety in a ternary structure having polypyridyl bases as additional photosensitizers and using the complexes as cellular imaging-cum-photochemotherapeutic agents. Vanadium being a bio-essential trace element, the oxovanadium(IV) complexes showing a low energy d-d band within the PDT spectral window (630-800 nm) are suitable as metal based PDT agents considering the greater tissue penetration of red light.<sup>24,25</sup> In continuation to our previous report,<sup>11</sup> we have now attempted to increase the aqueous solubility and cellular uptake of the complexes by derivatization of the OH groups of curcumin by glucose.<sup>26</sup> Cancer cells are known to have higher rates of glucose uptake due to decrease in oxidative phosphorylation and enhanced levels of glycolysis.<sup>27</sup> The pendant glucose moieties in the ternary structures are expected to enhance the cellular uptake of the complexes.<sup>28-30</sup> We have chosen planar phenanthroline bases (L), viz., 1,10-phenanthroline (phen) and dipyrido[3,2-a:2',3'-c]phenazine (dppz), for their intercalative DNA binding properties and the dppz ligand having a phenazine moiety for its photoactivity.

Herein, we present the synthesis, characterization, DNA binding, red light-induced DNA cleavage activity and visible light-induced cytotoxic properties of four oxovanadium(IV) complexes, viz. [VO(cur)(L)Cl] (L = phen, **1**; dppz, **2**) and [VO(scur)(L)Cl] (L = phen, **3**; dppz, **4**), where L is 1,10-phenanthroline (phen), dipyrido[3,2-a:2',3'-c]phenazine (dppz), cur is monoanionic curcumin and scur is monoanionic diglycosylcurcumin (Scheme 1). Complex [VO(cur)(phen)Cl] (**1**) has been structurally characterized by X-ray crystallography and the structural details are published in our preliminary communication.<sup>11</sup> Significant results of this study include remarkable enhancement in the photo-cytotoxicity and hydrolytic stability of curcumin on binding to an oxovanadium(IV) moiety. The complexes are less-toxic in dark. Cellular imaging of HeLa

and HaCaT cells shows mainly cytosolic localization of the complexes within 4 h of incubation and this observation is significant considering nuclear localization could possibly lead to undesirable mutation and carcinogenesis. The complexes show photoinduced cell cycle arrest in S and G2/M phase and cell death via apoptotic pathway. We have observed mitochondrial localization of complex **2**. This is of significance considering that the intrinsic pathway of apoptosis largely involves the mitochondria as is known for the PDT drug Photofrin®.

[Scheme 1]

## Results and discussion

### Synthesis and characterization

Oxovanadium(IV) complexes of curcumin and its derivative, viz. [VO(cur)(L)Cl] (**1**, **2**) and [VO(scur)(L)Cl] (**3**, **4**), having 1,10-phenanthroline (phen) or dipyrido[3,2-a:2',3'-c]phenazine (dppz) were synthesized in good yield from a general synthetic procedure in which vanadyl sulfate was first reacted with barium chloride in aqueous ethanol (1:5 v/v water-ethanol) and the filtrate after removal of barium sulfate was subsequently reacted with the respective phenanthroline base in ethanol followed by addition of curcumin (Hcur) or glycosylated curcumin (Hscur) in acetonitrile-ethanol mixture. The complexes were characterized from the spectroscopic and analytical data. Selected physicochemical data are given in Table 1. The ESI-MS of the complexes showed essentially a single peak corresponding to the [M-Cl]<sup>+</sup> in both MeCN and aqueous MeCN (Fig. S1-S4, ESI†). The mass spectral data suggest the stability of the five-coordinate complex as [VO(cur)(L)]Cl in the solution phase. The complexes gave molar conductance value of ~15 and ~95 S m<sup>2</sup> M<sup>-1</sup> in pure DMF and 10% aqueous DMF, respectively, suggesting their non-electrolytic behavior in DMF and 1:1 electrolytic nature in an aqueous medium due to dissociation of the chloride ligand.<sup>31</sup> The magnetic moment values of ~1.65  $\mu_B$  indicate the presence of the V(IV) oxidation state with one unpaired electron. The IR spectra of the complexes showed three bands near 1590, 1496 and 966 cm<sup>-1</sup> for the C=O, C=C ( $\beta$ -diketonate) and V=O stretching vibrations, respectively (Fig. S5, ESI†).<sup>32</sup> The IR-band at ~1590 cm<sup>-1</sup> (C=O stretching) indicates bidentate coordination mode of the  $\beta$ -diketone (cur/scur) ligand to the metal center. The oxovanadium(IV) complexes showed a broad and weak d-d band within 720–750 nm in 10% aqueous DMF (Fig. 1 (a)). The curcumin complexes (**1** and **2**) displayed an intense curcumin centered visible band at ~434 nm due to  $\pi \rightarrow \pi^*$  transition of the curcumin ligand with a shoulder at around 453 nm.<sup>33</sup> This band was observed at 424 nm with a shoulder at around 442 nm in diglycosylcurcumin complexes. This band could be utilized to photo-activate the complexes by visible light (400-700 nm) for generation of ROS which leads to cell death. The dppz ligand in the complexes showed an additional band near 360 nm assignable to the  $n \rightarrow \pi^*$  transition involving the phenazine moiety.<sup>34</sup> The other ligand-centered electronic spectral bands were observed in the UV region.

[Fig. 1]

The complexes in 10% aqueous DMSO on excitation at 420 nm exhibited green fluorescence at 510 nm with quantum yield

( $\phi$ ) values in the range of 0.01-0.02 (Fig. 1(b)). The curcumin ligand alone gave a  $\phi$  value of 0.04 under similar conditions. The curcumin based fluorescence is retained in the complexes and the emission spectral properties are suitable to study the cellular uptake and localization of the complexes inside the cells using confocal fluorescence microscopy. Glycosylation of curcumin has led to a blue-shift in both the absorption and emission band of the respective complexes in comparison to the curcumin complexes. The redox active complexes showed a reduction peak assignable to the V(IV)/V(III) couple near -1.2 V vs. SCE in 20% DMF-H<sub>2</sub>O with 0.1 M [Bu<sup>n</sup><sub>4</sub>N](ClO<sub>4</sub>) (TBAP) as the supporting electrolyte (Table 1, Fig. S6, ESI<sup>†</sup>). The complexes did not show any oxidative response. Redox stability of the complexes over a large potential window is expected to reduce their chemical nuclease activity and dark cellular toxicity.<sup>35</sup>

Computational studies were performed for the complexes using B3LYP/LANL2DZ level of DFT.<sup>36,37</sup> The energy optimised structures of the complexes showed a distorted octahedral structure with chelating *N,N*-donor phen or dppz, *O,O*-donor curcumin or diglycosylcurcumin monoanion and a chloride ligand (Fig. 2(a), Fig. S7, ESI<sup>†</sup>). The axial V=O bond distance is ~1.61 Å, while the other V-O bond distances are ~1.97 Å. It is evident from the optimised structure that the chloride ligand being at the *trans* position of the V=O is labile with a long V-Cl bond distance of ~2.61 Å. From the molecular orbital pictures it is observed that the HOMO is concentrated mostly over the curcumin moiety whereas the LUMO is located over the polypyridyl rings of the complexes **1**, **2** and **4** (Fig. 2(a), Fig. S8,S9, ESI<sup>†</sup>). Complex **3** has the HOMO based on curcumin with significant contribution from the chloride ligand and LUMO is located over the curcumin moiety (Fig. S10, ESI<sup>†</sup>). Complex **1** was structurally characterized earlier by single-crystal X-ray crystallography (Fig. 2(b)).<sup>11</sup> The oxovanadium(IV) complex has similar co-ordination mode as observed in the DFT optimised structure. The V=O bond distance is ~1.54 Å. The V-Cl bond *trans* to the V=O group is very long (~2.78 Å) and this labile bond is likely to get dissociated in an aqueous solution as is evidenced from the ESI-MS and molar conductivity data (Table 2).

[Fig. 2]

### Solubility and stability

The complexes showed good solubility in DMF and DMSO, moderate solubility in water, methanol, ethanol and acetonitrile, and poor solubility in hydrocarbons. The diglycosylcurcumin complexes **3** and **4** having carbohydrate moiety were soluble in water. Complex **1** showed solubility up to ~3.3 mg per ml of DMSO-10% DMEM medium (1:99 v/v, similar to cellular medium) at 25 °C. Complexes **2-4** in the same solvent composition gave solubility up to ~3.8, ~9.9 and ~10.2 mg per ml, respectively. The complexes were stable in the monocationic form on dissociation of the chloride ligand and the solution stability of the resulting cationic species was evidenced from the ESI-MS and the molar conductivity data. Curcumin alone is known to undergo hydrolysis in an aqueous buffer.<sup>11,19</sup> We have observed remarkable enhancement in the aqueous stability of curcumin as ligand on binding to the VO<sup>2+</sup> moiety in a buffer

medium. The absorption spectral study showed a gradual decrease in the absorption intensity of curcumin (Hcur) alone in a solution phase, while its VO<sup>2+</sup> complexes showed no apparent spectral change even after 48 h (Fig. S11, ESI<sup>†</sup>). The results indicate that co-ordination of curcumin to the VO<sup>2+</sup> moiety significantly increases its hydrolytic stability. This also provides a convenient way to deliver the drug into the target cells without its degradation under physiological conditions. This is likely to enhance the therapeutic potential of curcumin. The confocal images of curcumin alone showed its degradation over time resulting complete loss of its emission intensity. The metal complex, however, showed no apparent change in the emission intensity of the metal-bound curcumin ligand (Fig. S12, ESI<sup>†</sup>).

### Cellular incorporation assay

Cellular uptake studies were carried out to determine the incubation time of the complexes for *in-vitro* studies before exposure to visible light. Uptake of the complexes **2** and **4** in HaCaT, HeLa and MCF-7 cells at 2 and 4 h time points was studied by FACS (Fluorescence Activated Cell Sorter) analysis in which the fluorescence of the curcumin complexes were monitored (Fig. 3). The number of events in the upper left quadrant of the figure represents the population of cells in which the complex was not taken up and that in upper right quadrant represents the cell population with complex inside. The percentage incorporation of the complexes in the cells is also shown (Fig. S13, ESI<sup>†</sup>). On 2 h of incubation, uptake of the complexes was found to be more in HaCaT cells than in HeLa and MCF-7 cells. The results indicate different rates of cellular uptake of the complexes **2** and **4**. The uptake of the diglycosylcurcumin complex **4** is significantly higher (~100% on 4 h of incubation) compared to its curcumin analogue **2** (~83% at 4 h). This could be due to preferential internalization of the carbohydrate appended complex in cancer cells by the receptor mediated endocytosis.<sup>38</sup>

[Fig. 3]

We also performed experiments to demonstrate the active uptake of glucose functionalized complexes using **2** and **4**. Cells were first incubated with 10 mM glucose for 2 h followed by addition of the complexes. The results indicate that the percentage cellular uptake of the sugar appended complex **4** was significantly compromised from ~99.5% to ~40% upon incubation with excess glucose, whereas the percentage cellular uptake of the non-sugar complex **2** remained almost unaltered (Fig. 4(a), Fig. S14, ESI<sup>†</sup>). Moreover, the mean fluorescence intensity which demonstrates the mean compound uptake in cells was also significantly compromised for the sugar appended complex **4** in the presence of the added excess glucose while remaining same for complex **2** (Fig. 4(b), Fig. S15, ESI<sup>†</sup>). The enhanced uptake of complex **4** is indeed due to the introduction of the carbohydrate moiety and the internalization of complex **4** in the cancer cells is mainly through the receptor mediated endocytosis.

[Fig. 4]

### Cytotoxicity studies

The anticancer activity of the oxovanadium(IV) complexes

1-4, curcumin and its derivative was tested on HeLa and MCF-7 cancer cells as well as on immortalized HaCaT cells in dark and upon irradiation with a broadband visible light source (400-700 nm; Luzchem photoreactor, 10 J cm<sup>-2</sup>; irradiation time, 1 h). The complexes were incubated for 4 h and then irradiated with the visible light. Dark controls were used to measure the PDT effect. The extent of cytotoxicity was measured from the IC<sub>50</sub> values (50% inhibitory concentration) obtained from the MTT cell viability assay (Table 3, Fig. 5, Fig. S16-S21, ESI†).<sup>11,39</sup> The complexes were found to be remarkably photocytotoxic to all the cells studied and remained essentially nontoxic in dark. The IC<sub>50</sub> values of complex 1 were in the range of 6.4–10.0 μM. The values for complex 2 in light were within 2.3–4.7 μM. The higher photocytotoxicity of 2 than 1 is due to the presence of dipyrrophenazine as an additional photoactive moiety in 2. Complex 3 with a curcumin derivative having two sugar moieties gave IC<sub>50</sub> values within 3.5–5.8 μM. The reason for the higher photocytotoxicity of complex 3 than complex 1 could be due to higher cellular uptake in the presence of the sugar moieties. Complex 4, the most photoactive one, showed photo-cytotoxicity at nanomolar concentration giving IC<sub>50</sub> values within 0.63–2.4 μM, while being less cytotoxic in dark. A comparison of the IC<sub>50</sub> values of the complexes, the ligands, viz. curcumin and sugar-appended curcumin and other compounds is made in Table 3.<sup>40</sup> While curcumin showed moderate photocytotoxicity, its sugar derivative is not cytotoxic. Complexes showing photocytotoxicity in sub-micromolar concentration with minimal dark toxicity are of significance in the chemistry of PDT. The observed photocytotoxicity of the complexes 2–4 is comparable to that of the clinically approved PDT drug Photofrin®.<sup>41</sup> The present complexes having curcumin and its sugar derivative are potentially suitable for further studies in PDT.

[Fig. 5]

#### 35 Apoptosis: DNA ladder assay

DNA laddering is a convenient way to detect apoptotic cell death which results from the activation of endogenous endonucleases leading to degradation of genomic DNA into internucleosomal fragments of about 180 base pairs and its multiples. The DNA fragmentations can be analyzed by agarose gel electrophoresis giving a “ladder” like pattern at ~180 base pairs intervals. The alternate way of cell death is necrosis or direct damaged/fragmentation of genomic DNA by ROS and this is usually characterized by random DNA fragmentation giving “smear” pattern on agarose gels. The DNA laddering experiments were done for complexes 2 and 4 in HeLa and HaCaT cells. As shown in Fig. 6, it is evident that the complexes show ladder like pattern only after photo-irradiation in visible light of 400-700 nm (10 J cm<sup>-2</sup>; photo-irradiation time, 1 h) indicating apoptosis due to fragmentation of the genomic DNA as is reported for curcumin.<sup>33(b)</sup> However, no such DNA ladder was observed for the cells treated with the complexes in dark indicating that the light-induced cell death proceeds via apoptotic pathway.

[Fig. 6]

#### Apoptosis: annexin V-FITC/PI assay

To further confirm the apoptotic cell death induced by complex 4, we stained the cells that were pretreated with 3 μM of the complex for HeLa cells and 1 μM of the complex for HaCaT cells in dark and light with Annexin-V FITC and PI. Annexin-V, a calcium dependent protein, binds to phosphatidylserine exposed on the outer surface of the cells undergoing apoptosis due to membrane flipping in cells undergoing apoptosis. We have observed that complex 4 inducing apoptosis only on irradiation with visible light as the cells stained positive for Annexin-V indicating membrane flippage (Fig. 7). As shown in the figure, 48-65% of the cells were in an early apoptotic stage (positive for Annexin V staining), whereas the population of cells in necrosis mode (stained with PI) is significantly lower which again suggests the overall apoptotic mode of cell death.

[Fig. 7]

#### 75 DCFDA assay for ROS

The generation of any reactive oxygen species (ROS) by complex 4 was examined using visible light of 400-700 nm from dichlorofluorescein diacetate (DCFDA) assay in both HaCaT and HeLa cells. DCFDA is a cell permeable fluorogenic probe used for the detection of ROS in cells. It forms DCF on oxidation showing an emission maximum at 528 nm.<sup>42,43</sup> The fluorescence of DCF could be quantified from flow cytometry analysis. The cells treated with 4 in dark did not show any formation of DCF. However, cells treated with 4 on exposure to visible light for 1 h showed significant shift in the emission band towards right which indicates an increase in the intensity of emission resulting from the generation of DCF by the ROS-mediated oxidation of DCFDA (Fig. 8). The assay data in HaCaT and HeLa cells indicate the generation of ROS on exposure to visible light and this reactive species possibly causing cell apoptosis. There was no ROS formation observed in dark.

[Fig. 8]

#### Fluorescence microscopy

Fluorescence microscopy experiments were conducted for the complexes after 2 and 4 h incubation time in HeLa and HaCaT cells (Fig. 9). Dual staining was done to study any localization of the complexes inside the cell nucleus using propidium iodide (PI) which stains the nucleus. Merged images suggest mainly cytoplasmic localization of 1-4 in the HeLa and HaCaT cells (Fig. 9, Fig. S22, ESI† panel (c)). This observation is of significance considering nuclear localization of the drug being undesirable in PDT to avoid any potential damage to the nuclear DNA leading to mutation and carcinogenesis. It is apparent from the microscopy data that the complexes enter into the cells within 2 h and uptake of the complex increases in 4 h (Fig. S23, ESI†). As mentioned above, free curcumin in HeLa cells showed only little green fluorescence in 2 h and there was no visible fluorescence intensity after 4 h (Fig. S12, ESI†). This suggests degradation of curcumin (Hcur) in a cellular medium. The stability of curcumin gets significantly enhanced on binding to the oxovanadium(IV) moiety as observed from the microscopy data of the complexes (Fig. 9). The intra-cellular fluorescence intensity of the sugar appended complexes 3 and 4 is significantly higher compared to their normal analogue.

[Fig. 9]

To visualise the PDT effect, complexes **2** (5  $\mu\text{M}$ ) and **4** (3  $\mu\text{M}$ ) were added to the HaCaT cells and after incubation for 4 h, cells were exposed to visible light of 400-700 nm. Fluorescence images after 1 h light exposure displayed irregular nuclear morphology on staining with PI (Fig. 10, panels (c)). Chromatin condensation of the nucleus was observed indicating apoptotic cell death as bright condensed nuclei were seen in the cells (panels (c)). The PI staining revealed that the nuclear morphology remained unchanged in dark indicating non-cytotoxic nature of the complexes in dark. The microscopy data suggest that the complexes remain harmless inside the cells in dark and damage the cancer cells only upon photo-irradiation.

[Fig. 10]

### 15 Targeting mitochondria

With the knowledge that the complexes get accumulated primarily in the cytoplasm of the HeLa and HaCaT cells, we probed for any specific localization of the complexes to the cellular organelle. For this purpose, we have chosen complexes **2** and **4** giving green fluorescence and did dual staining with mitotracker deep red which stains only the mitochondria. The data showed complexes **2** and **4** co-localizing with the mitotracker in a significant manner on 4 h of incubation as is evident from the merged images shown in panels (c) of Fig. 11. Complexes localizing in mitochondria are of significance since mitochondria plays the key role in the intrinsic pathway of apoptosis. Thus any changes in the cancer cells leading to protection from apoptosis could be targeted. Photofrin<sup>®</sup> is known to localize in the mitochondria for its activity.<sup>44</sup>

[Fig. 11]

### Cell cycle profiling

Cell cycle analysis was performed for complexes **2** and **4** to study their effect on the cell cycle profile, if any. The analysis was done in three cell lines, viz., MCF-7, HaCaT and HeLa, by treating them with the complexes **2** and **4** in dark and light (400-700 nm; irradiation time, 1 h). No change in the cell cycle profile was observed in this visible light with respect to dark control indicating that this range of light is not inducing any cell cycle arrest or cell death. Complex **4** showed arrest in S and G2/M phases in MCF-7 and HaCaT cells, while a distinct sub G1 population was obtained in HeLa cells on 7 h of incubation after light irradiation. Complex **2** arrested MCF-7 cells predominantly in the S phase. In HaCaT and HeLa cells, S phase and G2/M arrest could be seen under same experimental conditions (Fig. 12, Fig. S24-S26, ESI<sup>†</sup>). Cell cycle profiles remained similar to that of the control for both the complexes in dark in all the three cell lines.

[Fig. 12]

### DNA binding and cleavage

As evidenced from the confocal microscopy study, the complexes localize mainly in the cytoplasm and significantly in the mitochondria. This suggests that the mitochondrial DNA could be a potential target of the complexes. The DNA binding

and cleavage activity of the complexes are thus of importance to understand their cellular activity. The binding affinity of the complexes to calf thymus (ct) DNA was studied by spectral and hydrodynamic methods (Table 1). The absorption spectral technique was used to determine the intrinsic binding constant ( $K_b$ ) value of the complexes by monitoring the decrease in the absorption of the curcumin centered bands near 430 nm. The  $K_b$  values range from  $6.1(\pm 0.4) \times 10^4$  to  $7.2(\pm 0.2) \times 10^5 \text{ M}^{-1}$  giving an order of the DNA binding strengths: **4** > **2** > **3** > **1** (Fig. S27, ESI<sup>†</sup>). The planarity of the dppz ligand makes its complexes better binders to ct-DNA than their analogues. DNA melting studies in phosphate buffer (pH 7.2) showed stabilizing interaction of the complexes with ct-DNA (Table 1, Fig. S28, ESI<sup>†</sup>). The  $\Delta T_m$  value for curcumin (Hcur) is 0.9 °C while the values for the complexes lie within 6.9 to 2.0 °C. It is 10.6 °C for the classical DNA intercalator ethidium bromide (EB).<sup>45</sup> The DNA melting data gave a similar order indicating intercalative mode of binding of the dppz complexes to the ct-DNA. A similar order is also obtained from the viscosity study. EB as a DNA intercalator and Hoechst dye as a groove binder were used as references. The plots of  $(\eta/\eta_0)^{1/3}$  vs. [complex]/[DNA] ratio showed partial intercalative binding mode of the complexes **2** and **3** to ct-DNA (Fig. S29, ESI<sup>†</sup>). Complex **1** showed primarily groove binding propensity, while complex **4** having scur and dppz ligands exhibited a similar plot as observed for the EB suggesting significant intercalative nature of DNA binding of this complex.

The DNA photocleavage activity of the complexes was studied using supercoiled (SC) pUC19 DNA in Tris-HCl/NaCl buffer upon irradiation with near-IR light of 705 and 785 nm using diode lasers (Table 4, Fig. S30-S32, ESI<sup>†</sup>). The choice of these wavelengths is based on the presence of a d-d band within 720-750 nm in the electronic spectra. The phen complexes **1** and **3** showed only moderate DNA photocleavage activity due to presence of monoanionic curcumin as the only photosensitizer. Complexes **2** and **4** having photoactive phenazine moiety showed very efficient photocleavage of DNA. A 40  $\mu\text{M}$  solution of these complexes gave essentially complete cleavage of plasmid DNA (~90%) from its SC to nicked circular (NC) form on 1.0 h photo-exposure time. Control experiments in dark did not show any significant DNA cleavage activity of the complexes and the ligands. The curcumin dye alone showed ~11% cleavage of SC DNA in dark. This could be due to generation of reactive oxygen species in an aqueous solution of curcumin.<sup>33</sup> Curcumin as a photosensitizer showed ~16% cleavage of SC DNA. The cleavage activity of curcumin gets remarkably enhanced on binding to the metal possibly due to efficient intersystem crossing (ISC).<sup>46</sup> The overall results indicate that the photo-excitation is metal-assisted involving the d-d band forming an excited state that generates the cleavage active species.<sup>21,24</sup>

The DNA groove binding propensity of the complexes was studied using distamycin-A as a minor groove binder (50  $\mu\text{M}$ ) and methyl green (25  $\mu\text{M}$ ) as a major groove binder (Fig. S33, ESI<sup>†</sup>).<sup>47,48</sup> Distamycin-A or methyl green alone showed ~18% cleavage of SC DNA in red light of 785 nm for 1.0 h exposure time. Addition of **1-4** to the distamycin-A bound SC DNA showed no apparent decrease in the DNA photo-cleavage activity. However, the complexes showed significant inhibition in

the DNA cleavage activity for methyl green bound SC DNA suggesting major groove binding nature of these complexes in preference to the minor groove. The complexes did not show any significant photocleavage of DNA in red light under argon as an inert atmosphere indicating the necessity of molecular oxygen to generate the cleavage active species (Fig. S34, ESI†). The DNA cleavage reactions involving molecular oxygen ( $^3\text{O}_2$ ) could proceed via two major mechanistic pathways. The excited electronic state of the complex through efficient intersystem crossing (ISC) could generate an excited state that can activate molecular oxygen to its reactive singlet ( $^1\text{O}_2$ ,  $^1\Delta_g$ ) state by energy transfer in a type-II process.<sup>5,49</sup> In an alternate pathway, the redox active photo-activated complex could reduce molecular oxygen to generate reactive hydroxyl radical species by a photo-redox mechanism.<sup>50</sup> We have observed that singlet oxygen quenchers, viz. TEMP and sodium azide showed no apparent effect on the DNA cleavage activity thus ruling out the possibility of a type-II singlet oxygen pathway. Significant inhibition in the DNA cleavage was observed in the presence of  $\cdot\text{OH}$  scavengers, viz. DMSO, KI and catalase indicating presence of a photo-redox pathway. The involvement of superoxide radical intermediate was evidenced from the inhibitory role of SOD as an additive. Although the precise mechanistic details are not well understood, the photo-activated oxovanadium(IV) complexes in red light seem to reduce the metal ion forming reactive V(III) species that forms hydroxyl radicals following a Fenton-like mechanism which is known for the copper-dipyridoquinoxaline and iron-bleomycin species.<sup>51</sup> The formation of hydroxyl radicals is also evidenced from the EPR data using DMPO (5,5-dimethyl-1-pyrroline N-oxide) as a stabilizer showing the characteristic four line spectra of DMPO- $\cdot\text{OH}$  adduct upon irradiation of complex 4 with red light of 785 nm for 1.0 h (Fig. S35, ESI†).<sup>52</sup>

## Experimental

### Materials

All reagents and chemicals were procured from commercial sources (s.d. Fine Chemicals, India; Aldrich, USA) and used as such without further purification. Curcumin (95% curcuminoid content, 80% curcumin (Hcur)) was purchased from Sigma-Aldrich and purified into individual components by following a reported procedure.<sup>53</sup> Solvents were purified by standard procedures.<sup>54</sup> Supercoiled (SC) pUC19 DNA (cesium chloride purified) was purchased from Bangalore Genie (India). Tris-(hydroxymethyl)aminomethane-HCl (Tris-HCl) buffer solution was prepared using deionized and sonicated triple distilled water. Calf thymus (ct) DNA, agarose (molecular biology grade), distamycin-A, catalase, superoxide dismutase (SOD), 2,2,6,6-tetramethyl-4-piperidone (TEMP), 2',7'-dichlorofluorescein diacetate (DCFDA), Hoechst 33258, ethidium bromide (EB), propidium iodide (PI), 3-(4,5-dimethylthiazol-2-yl)-2,5-diphenyltetrazolium bromide (MTT), Dulbecco's modified eagle medium (DMEM), Dulbecco's phosphate buffered saline (DPBS) and fetal bovine serum (FBS) were purchased from Sigma (USA). MitoTracker<sup>®</sup> Deep Red FM (Cat. no.M22426) (MTR) was purchased from Invitrogen Bio Services, India. Dipyrido[3,2-a:2',3'-c]phenazine (dppz) was prepared following a literature

procedure using 1,10-phenanthroline-5,6-dione as a precursor.<sup>55</sup> The glycosylated curcumin derivative, viz., diglycosylcurcumin (Hscur, 1,7-bis(3-methoxy-4- $\beta$ -D-glucopyranos-1-yl)oxyphenyl)hepta-1,6-diene-3,5-dione), was prepared according to a literature method (Fig. S36, ESI†).<sup>26</sup> Synthesis of the complexes was carried out under nitrogen atmosphere using Schlenk technique. Tetrabutylammonium perchlorate (TBAP) was prepared using tetrabutylammonium bromide and perchloric acid.

### Measurements

The elemental analysis was done using a Thermo Finnigan FLASH EA 1112 CHNS analyzer. The infrared, electronic spectra were recorded on Perkin-Elmer Lambda 35 and Perkin-Elmer spectrum one 55, respectively, at 25 °C. Molar conductivity measurements were done using a Control Dynamics (India) conductivity meter. Electrochemical measurements were made at 25 °C on an EG&G PAR model 253 VersaStat potentiostat/galvanostat with electrochemical analysis software 270 using a three electrode setup consisting of a glassy carbon working, platinum wire auxiliary and a saturated calomel reference electrode (SCE) in 20% DMF-H<sub>2</sub>O. TBAP (0.1 M) was used as a supporting electrolyte for the electrochemical measurements. The electrochemical data were uncorrected for junction potentials. Electrospray ionization (ESI) mass spectral measurements were made using Agilent Technologies 6538 UHD Accurate-mass Q-TOF LC/MS and Bruker Daltonics make Esquire 300 Plus ESI model mass spectrometers. Room temperature fluorescence quantum yield measurements were done using a Perkin-Elmer LS 55 fluorescence spectrometer using coumarin-153 laser dye as a reference with a known  $\Phi$  value of 0.56.<sup>56</sup> Samples were deaerated prior to the spectral measurements. The complexes and the reference were excited at 420 nm. Nearly equal absorbance and the emission spectra were recorded from 450 to 600 nm. The integrated emission intensity was calculated using Origin Pro 8.1 software and the quantum yield was calculated from the equation:  $(\Phi_S/\Phi_R) = (A_S/A_R) \times ((OD)_S/(OD)_R) \times (n_S^2/n_R^2)$ , where,  $\Phi_S$  and  $\Phi_R$  are the fluorescence quantum yields of the sample and reference, respectively,  $A_S$  and  $A_R$  are the area under the fluorescence spectra of the sample and the reference respectively,  $(OD)_S$  and  $(OD)_R$  are the respective optical densities of the sample and the reference solution at the wavelength of excitation, and  $n_S$  and  $n_R$  are the refractive indices for the respective solvents used for the sample and the reference.<sup>57,58</sup> The NMR spectra were recorded using Bruker Avance 400 NMR spectrometer (400 MHz). Magnetic susceptibility measurements at 298 K were carried out with solid sample using MPMS SQUID VSM (Quantum Design, USA). Vanadium metal was estimated using an Inductively Coupled Plasma Mass Spectrometer (ICPMS, Thermo X Series II). EPR spectral study was carried out with a Bruker ER200D spectrometer. Viscometric measurements were performed with a Schott AVS 310 automated viscometer. Confocal microscopy was done using Olympus IX 81 fluorescence microscope. Flow cytometric analysis was performed using FACS Calibur (Becton Dickinson (BD) cell analyzer) at FL2 channel (595 nm).

## Syntheses

Vanadyl sulfate (0.16 g, 1.0 mmol) and barium chloride (0.24 g, 1.0 mmol) together were dissolved in 15 ml of ethanol and 3 ml of water. The mixture was then stirred at room temperature for 1.5 h under nitrogen atmosphere using Schlenk technique. The mixture was filtered using celite to remove white barium sulphate as the precipitate. The blue filtrate was deaerated and then saturated with nitrogen. An ethanol solution (10 ml) of the corresponding phenanthroline base (0.19 g, phen; 0.28 g, dppz, (1.0 mmol)) was added to the filtrate. A deep greenish solution was formed after stirring the mixture for 20 min. To this mixture was added a deaerated ethanol solution (15 ml) of the  $\beta$ -diketone ligand (0.36 g, Hcur; 0.69 g, Hscur (1.0 mmol)) which was previously neutralized with  $\text{Et}_3\text{N}$  (0.10 g, 1.0 mmol). The complexes were precipitated out of the solution spontaneously as solid after stirring for 1 h. The precipitate was then filtered, isolated and washed with ethanol, THF and chloroform and finally dried in vacuum over  $\text{P}_4\text{O}_{10}$ .

**Complex 1:** Yield = 87%. Anal. Calcd for  $\text{C}_{33}\text{H}_{27}\text{N}_2\text{ClO}_7\text{V}$ : C, 60.98; H, 4.19; N, 4.31; V, 7.84. Found: C, 60.79; H, 4.26; N, 4.21; V, 7.91. ESI-MS in  $\text{CH}_3\text{CN}$ :  $m/z$  614.1125  $[\text{M}-\text{Cl}]^+$ . IR data/  $\text{cm}^{-1}$ : 3064 w, 1590 s, 1491 vs, 1420 s, 1381 m, 1276 s, 1152 m, 1122 m, 1035 w, 966 m, 840 m, 720 m, 555 w, 460 w (vs, very strong; s, strong; m, medium; w, weak). UV-visible in 10% DMF [ $\lambda_{\text{max}}/\text{nm}$  ( $\epsilon/\text{dm}^3 \text{mol}^{-1} \text{cm}^{-1}$ ): 721 (54), 453 sh (33000), 434 (35600), 265 (30400)]. Molar conductivity in 10% aqueous DMF at 298 K [ $\Lambda_{\text{M}}/\text{S cm}^2 \text{mol}^{-1}$ ]: 104.  $\mu_{\text{eff}}$ ;  $\mu_{\text{B}}$  at 298 K: 1.67.

**Complex 2:** Yield = 74%. Anal. Calcd for  $\text{C}_{39}\text{H}_{29}\text{N}_4\text{ClO}_7\text{V}$ : C, 62.28; H, 3.89; N, 7.45; V, 6.77. Found: C, 62.41; H, 3.77; N, 7.42; V, 6.69. ESI-MS in  $\text{CH}_3\text{CN}$ :  $m/z$  716.1363  $[\text{M}-\text{Cl}]^+$ , IR data/  $\text{cm}^{-1}$ : 3070 w, 1587 s, 1490 vs, 1422 s, 1377 m, 1279 s, 1154 m, 1117 m, 1031 w, 968 m, 810 m, 723 m, 558 w, 463 w, 435 m. UV-visible in 10% DMF [ $\lambda_{\text{max}}/\text{nm}$  ( $\epsilon/\text{dm}^3 \text{mol}^{-1} \text{cm}^{-1}$ ): 731 (64), 454 sh (38600), 434 (43900), 382 (25600), 361 (20300), 268 (46600)]. Molar conductivity in 10% aqueous DMF at 298 K [ $\Lambda_{\text{M}}/\text{S cm}^2 \text{mol}^{-1}$ ]: 96.  $\mu_{\text{eff}}$ ;  $\mu_{\text{B}}$  at 298 K: 1.61.

**Complex 3:** Yield = 81%. Anal. Calcd for  $\text{C}_{45}\text{H}_{47}\text{N}_2\text{ClO}_{17}\text{V}$ : C, 55.48; H, 4.86; N, 2.88; V, 5.23. Found: C, 55.61; H, 4.79; N, 2.85; V, 5.26. ESI-MS in  $\text{CH}_3\text{CN}$ :  $m/z$  938.20  $[\text{M}-\text{Cl}]^+$ , IR data/  $\text{cm}^{-1}$ : 3310 m (br), 1585 s, 1502 vs, 1421 m, 1361 m, 1255 s, 1122 m, 1071 m, 1026 m, 964 m, 816 w, 730 m, 540 w, 469 w (br, broad). UV-visible in 10% DMF [ $\lambda_{\text{max}}/\text{nm}$  ( $\epsilon/\text{dm}^3 \text{mol}^{-1} \text{cm}^{-1}$ ): 752 (55), 439 sh (29600), 420 (36800), 270 (38000)]. Molar conductivity in 10% aqueous DMF at 298 K [ $\Lambda_{\text{M}}/\text{S cm}^2 \text{mol}^{-1}$ ]: 90.  $\mu_{\text{eff}}$ ;  $\mu_{\text{B}}$  at 298 K: 1.69.

**Complex 4:** Yield = 79%. Anal. Calcd for  $\text{C}_{51}\text{H}_{49}\text{N}_4\text{ClO}_{17}\text{V}$ : C, 56.91; H, 4.59; N, 5.21; V, 4.73. Found: C, 56.83; H, 4.64; N, 5.30; V, 4.75. ESI-MS in  $\text{CH}_3\text{CN}$ :  $m/z$  1040.2452  $[\text{M}-\text{Cl}]^+$ , IR data/  $\text{cm}^{-1}$ : 3303 m (br), 1588 s, 1503 vs, 1422 w, 1383 w, 1276 s, 1124 m, 1070 m, 1029 m, 961 m, 818 w, 726 w, 550 w, 467 w. UV-visible in 10% DMF [ $\lambda_{\text{max}}/\text{nm}$  ( $\epsilon/\text{dm}^3 \text{mol}^{-1} \text{cm}^{-1}$ ): 749 (67), 444 sh (35600), 426 (41200), 381 (31600), 362 (26500), 267

(54700)]. Molar conductivity in 10% aqueous DMF at 298 K [ $\Lambda_{\text{M}}/\text{S cm}^2 \text{mol}^{-1}$ ]: 87.  $\mu_{\text{eff}}$ ;  $\mu_{\text{B}}$  at 298 K: 1.64.

## X-ray crystallographic procedures

The crystal structure of complex **1** was obtained by using the single-crystal X-ray diffraction technique. Crystals were grown on slow evaporation of the solvent of an acetonitrile solution of the complex. Crystal mounting was done on glass fibre with epoxy cement. All geometric and intensity data were collected at low temperature (100 K) using an automated Bruker SMART APEX CCD diffractometer equipped with a fine focus 1.75 kW sealed tube Mo- $\text{K}\alpha$  X-ray source ( $\lambda = 0.71073 \text{ \AA}$ ) with increasing  $\omega$  (width of  $0.3^\circ$  per frame) at a scan speed of 5 sec per frame. Intensity data, collected using  $\omega$ - $2\theta$  scan mode, were corrected for Lorentz-polarization effects and for absorption.<sup>59</sup> The structure was solved and refined using SHELXL97 present in the WinGx suit of programs (Version 1.63.04a).<sup>60,61</sup> All non-hydrogen atoms were initially located in the difference Fourier maps, and for the final refinement, the hydrogen atoms were placed in geometrically ideal positions and refined in the riding mode. Final refinement included atomic positions for all the atoms, anisotropic thermal parameters for all the non-hydrogen atoms and isotropic thermal parameters for all the hydrogen atoms. The electron density contributions from the highly disordered solvent molecules were removed using the SQUEEZE routine (PLATON).<sup>62</sup> EADP restraint was used on the atoms C25 and C27 in order to avoid eccentric thermal ellipsoids.

Crystal data for **1**:  $\text{C}_{33}\text{H}_{27}\text{ClN}_2\text{O}_7\text{V}$ ,  $M = 649.96$ , triclinic,  $P\bar{1}$ ,  $a = 9.3606(11)$ ,  $b = 12.8152(18)$ ,  $c = 16.3781(19) \text{ \AA}$ ,  $\alpha = 102.249(11)$ ,  $\beta = 101.851(10)$ ,  $\gamma = 104.124(11)^\circ$ ,  $U = 1792.1(4) \text{ \AA}^3$ ,  $Z = 2$ ,  $D_c = 1.205 \text{ Mg m}^{-3}$ ,  $T = 293(2) \text{ K}$ , reflections collected/unique [ $R(\text{int})$ ]: 24877/6004 [0.1291],  $F(000) = 670$ , GOOF = 0.912,  $R1[wR2] = 0.1050$  [0.2340] for 6004 reflections [ $I > 2\sigma(I)$ ] and 385 parameters [ $R1(F^2) = 0.1775$  (all data)]. The CCDC deposition number is 882736.

## Cellular incorporation assay

Flow cytometric analysis was performed to study uptake of the complexes **2** and **4** in HeLa, HaCaT and MCF-7 cells. Approximately  $0.3 \times 10^6$  cells were plated per well of a 6-well tissue culture plate in DMEM containing 10% FBS. After 24 h of incubation at  $37^\circ\text{C}$  in a  $\text{CO}_2$  incubator, complexes **2** and **4** (10  $\mu\text{M}$ ) were added to the cells at different incubation time intervals (2 and 4 h) in dark. Then the cells were trypsinized, transferred into 1.5 ml centrifuge tubes, washed once with chilled PBS centrifuging at 4000 rpm for 5 min at  $4^\circ\text{C}$ . The supernatant was discarded and the cell pellet was suspended in 200  $\mu\text{l}$  of PBS. Flow cytometric analysis was performed using FACS Calibur (Becton Dickinson (BD) cell analyzer) at FL-2 channel. For confirming that complex **4** was taken up by cells mainly through glucose receptor mediated endocytosis, HeLa cells were first incubated with 10 mM glucose for 2 h with subsequent addition of complexes **2** and **4** for the FACS analysis.

## Cell cytotoxicity assay

Photocytotoxicity of the complexes **1-4** was assessed from MTT assay in which mitochondrial reductases in viable cells cleave the tetrazolium rings of MTT forming dark blue membrane impermeable crystals of formazan which can be dissolved in DMSO and estimated from spectral measurements at 530 nm.<sup>39</sup> The quantity of formazan formed gave a measure of the number of viable cells. HeLa, HaCaT and MCF-7 cells were used to carry out the MTT assay. About 8000 cells were taken in each well of a 96-well culture plate in DMEM containing 10% FBS. After 24 h of incubation at 37 °C in a CO<sub>2</sub> incubator, different concentrations (50, 25, 12.5, 6.25, 3.12 and 1.56 μM in HeLa; 50, 25, 12.5, 6.25, 3.12, 1.56 and 0.78 μM in MCF-7 and HaCaT) of the complexes dissolved in 1% DMSO -DMEM were added to the cells and incubation was continued for a period of 4 h in dark. The medium was subsequently replaced with PBS and photo-irradiation was done in visible light of 400-700 nm (10 J cm<sup>-2</sup>; irradiation time; 1 h) using Luzchem Photoreactor (Model LZC-1, Ontario, Canada) fitted with Sylvania make 8 fluorescent white tubes with a fluence rate of 2.4 mW cm<sup>-2</sup>. Post irradiation, PBS was replaced with DMEM-FBS and incubation was continued for a further period of 20 h in dark. After incubation, a 25 μl of 4 mg ml<sup>-1</sup> of MTT was added to each well and incubation was done for an additional 4 h. The culture medium was subsequently discarded and 100 μl of DMSO was added to dissolve the formazan crystals. The absorbance was determined using a BIORAD ELISA plate reader. The cytotoxicity of the complexes was measured as the percentage ratio of the absorbance of the compound treated with the cells and light irradiation to that of the irradiated cells in absence of the compound as a light control. The IC<sub>50</sub> values of the complexes were determined by a nonlinear regression analysis “log(inhibitor) vs. normalised response (variable slope)” using the GraphPad Prism 5.1.<sup>63</sup>

#### DNA fragmentation analysis

DNA fragmentation analysis by agarose gel electrophoresis was performed to determine the cell death mechanism induced by complexes **2** and **4**. Briefly, 3.0x10<sup>5</sup> HaCaT or HeLa cells were taken in each 60 mm dish. It was grown for 24 h and later treated with **2** (4 μM in HaCaT and 5 μM in HeLa) and **4** (1 μM in HaCaT and 3 μM in HeLa) and incubated for 4 h in dark. One dish containing the complex was exposed to light for 1 h and again the cells were left to grow for 4 h along with its dark control in another dish. After 4 h, cells were trypsinized, washed with DPBS and re-suspended in 0.4 ml of lysis buffer (10 mM Tris-HCl; pH, 8.0, 20 mM EDTA, 0.2% triton-X 100) for an incubation time of 20 min on ice. Lysed cells were centrifuged for 20 min at 13000 rpm and their supernatant having soluble chromosomal DNAs including both high molecular weight DNA and nucleosomal DNA fragments was collected. Phenol:chloroform (1:1) was added and centrifuged again at 13000 rpm for 20 min to remove the protein present. Later, supernatant was precipitated with 1/10 volume of 3M sodium acetate (pH, 5.8) and 2 volume of ethanol at -20 °C for overnight. DNA pellet was washed with 70% alcohol and re-suspended in Tris-EDTA (pH = 8) containing RNase (100 μg ml<sup>-1</sup>

<sup>1</sup> RNase) followed by incubation at 37 °C for 2 h. DNA samples were resolved on 1.5% agarose gel at 80 V for ~2 h and photographed under UV light.

#### Annexin-V FITC and PI assay

To ascertain the apoptotic pathway of cell death, HeLa and HaCaT cells (4 x 10<sup>5</sup> cells ml<sup>-1</sup>) were treated with complex **4** (3 μM in HeLa and 1 μM in HaCaT) in 10% DMEM for 4 h, followed by exposure to visible light for 1 h. The cells were then cultured for 18 h in complete medium, harvested and washed twice with chilled PBS at 4 °C. The cells were re-suspended in 200 μl Annexin-V binding buffer (100 mmol HEPES/ NaOH, pH of 7.4 containing 140 mM NaCl and 2.5 mM CaCl<sub>2</sub>), stained with Annexin-V FITC and PI, and incubated for 15 min in dark. After incubation the cells were analyzed immediately using flow cytometry.<sup>64</sup>

#### ROS from DCFDA assay

The generation of ROS was probed using 2',7'-dichlorodihydrofluorescein diacetate (DCFDA) assay.<sup>38</sup> Cell permeable DCFDA gets oxidized by cellular ROS to generate fluorescent DCF with an emission maxima at 525 nm. The percentage of cells generating ROS can be determined by flow cytometry analysis. To detect any ROS generation, HeLa and HaCaT cells were incubated with complex **4** (3 μM in HeLa and 1 μM in HaCaT) for 4 h followed by photo-irradiation (400-700 nm) for 1 h in 50 mM PBS. The cells were harvested by trypsinization and single cell suspension of 1x10<sup>6</sup> cells ml<sup>-1</sup> was prepared. The cells were then treated with 10 μM DCFDA solution in DMSO in dark for 15 min at room temperature. The distribution of DCFDA stained HeLa and HaCaT cells was determined by flow cytometry.

#### Confocal experiments

Uptake of the fluorescent complexes **1-4** and curcumin (Hcur) into the cells was visualized using a confocal scanning electron microscope (Zeiss, LSM510 apocromat). HaCaT and HeLa cells were grown on glass cover slips in each 12 well plates at a seeding density of 5x10<sup>4</sup> cells in 1.5 ml of culture medium for 24 h. Cells were then treated with the complexes (10 μM) for 2 and 4 h in dark. Cells were fixed and permeabilized with chilled methanol for 5 min at -20 °C. Methanol was subsequently removed followed by washing with 1X PBS. It was later incubated with propidium iodide (1 mg ml<sup>-1</sup>) for 2 min to stain the nucleus and visualized under a confocal scanning electron microscope. To view the PDT effect we performed the experiments with complexes **2** (5 μM) and **4** (3 μM) by exposing one of the HaCaT cell plate to visible light for 1 h. The cell-permeant MitoTracker<sup>®</sup> deep red having a mildly thiol-reactive chloromethyl moiety was used for labeling mitochondria on live non fixed cells. A 50 nM of MitoTracker<sup>®</sup> Deep Red FM (Cat. no.M22426) was used for confocal microscopy.

#### FACS for cell cycle profiling

To study the effect of the complexes **2** and **4** on the cell cycle,  $\sim 3 \times 10^5$  HeLa, HaCaT and MCF-7 cells were plated per well of a 6-well tissue culture plate in DMEM containing 10% FBS. After 24 h of incubation at 37 °C in a CO<sub>2</sub> incubator, samples with various concentrations of **2** and **4** in 1% DMSO buffer were added to the cells and incubation was continued for 4 h in dark. The medium was subsequently replaced with PBS and photo-irradiation was done in visible light (400–700 nm) using Luzchem Photoreactor for 1 h. After photoexposure, PBS was removed and replaced with DMEM-10% FBS and incubation was continued for another period of 7 h in dark. After incubation, cells were trypsinized and collected into 1.5 ml centrifuge tubes. The cells were washed once with chilled PBS of pH 7.4 and fixed by adding 800  $\mu$ l of chilled 70% ethanol drop-wise with constant and gentle vortexing to prevent aggregation of cells. The cell suspension was incubated at -20 °C for 6 h. The fixed cells were then washed twice with 1.0 ml of chilled PBS by centrifuging at 4000 rpm for 5 min at 4 °C. The supernatant was discarded by gently inverting the tube and the cell pellet was suspended in 200  $\mu$ l of PBS containing 10  $\mu$ g ml<sup>-1</sup> DNase-free RNase for 12 h period at 37 °C for digesting the cellular RNA. After digestion, a 20  $\mu$ l volume of 1.0 mg ml<sup>-1</sup> propidium iodide solution was added into the mix and incubated further for 20 min at 25 °C in dark. Flow cytometric analysis was performed using FACS Calibur (Becton Dickinson “Cell Quest Pro” software) cell analyzer at FL2 channel (595 nm). Data analysis was performed for the percentage of cells in each cell cycle phase by using WinMDI version 3.1.<sup>65</sup>

### DNA binding experiments

The DNA binding experiments were carried out using calf thymus (ct) DNA in Tris-HCl buffer (50 mM Tris- HCl, pH = 7.2) at room temperature by following the procedures reported earlier from our group.<sup>24</sup> The intrinsic equilibrium binding constants ( $K_b$ ) of the complexes to ct-DNA were obtained by McGhee-von Hippel (MvH) method using the expression of Bard and co-workers.<sup>66,67</sup> DNA melting experiments were done by monitoring the absorption intensity of ct-DNA at 260 nm at various temperatures, both in the absence and presence of the oxovanadium(IV) complexes. Measurements were made using a Perkin-Elmer Lambda 35 spectrophotometer equipped with a Peltier temperature-controlling programmer (PTP 6) ( $\pm 0.1$  °C) on increasing the temperature of the solution by 0.5 °C min<sup>-1</sup>. The viscosity measurements were done using Schott Gerate AVS 310 automated viscometer attached with constant temperature bath at 37( $\pm 0.1$ ) °C. The concentration of ct-DNA stock solution was 150  $\mu$ M (NP) in 5 mM Tris-HCl buffer. The complex was added gradually on increasing the concentration from 0 to 120  $\mu$ M, and the viscosity was measured on each addition. The flow times were monitored with an automated timer. The relative specific viscosity of DNA,  $(\eta/\eta_0)^{1/3}$  was plotted *versus* [complex]/[DNA], where  $\eta$  is the viscosity of DNA in the presence of the complex and  $\eta_0$  is the viscosity of ct-DNA alone in 5 mM Tris buffer medium. The viscosity values were calculated from the observed flow time of the ct-DNA containing solutions ( $t$ ), after correcting for that of the buffer alone ( $t_0$ ),  $\eta = (t - t_0)/t_0$ . Due corrections were made for the viscosity of DMF solvent present in the

solution.

### DNA cleavage experiments

The photo-cleavage of supercoiled pUC19 DNA (0.2  $\mu$ g, 50  $\mu$ M, 2686 base-pairs) was studied by agarose gel electrophoresis using the complexes **1-4** (40  $\mu$ M) in 50 mM Tris-HCl buffer of pH 7.2 and 50 mM NaCl containing 10% DMF. The photo-excitation was carried out in near-IR red light using diode lasers of 705 nm and 785 nm wavelengths (Model: LQC705-38E and LQC785-100C from Newport Corporation with LD module, continuous-wave (CW) elliptical beam and circular beam, respectively). The laser powers were 38 and 100 mW, respectively, measured using Spectra Physics CW laser power meter (Model 407A). Each sample was pre-incubated for 1.0 h at 37 °C in dark and then exposed to light. After light exposure, each sample was further incubated for 1.0 h at 37 °C in dark followed by addition of the loading dye (25% bromophenol blue, 0.25% xylene cyanol and 30% glycerol (2  $\mu$ l)), and finally loaded on a 1% agarose gel containing 1  $\mu$ g ml<sup>-1</sup> of ethidium bromide (EB). The gels were run at 50 V for  $\sim 2$  h in TAE buffer. The bands were visualized in UV light, photographed, and the intensities of the bands measured using the UVITECH Gel Documentation System. Due corrections were made for the trace amount of NC form present in the SC DNA and the higher affinity of EB for binding to NC and linear forms of DNA over the SC form.<sup>68</sup> The error in measuring the band intensities was  $\sim 5\%$ . The mechanistic studies were carried out using different additives (NaN<sub>3</sub>, 0.5 mM; TEMP, 0.5 mM; DMSO, 4  $\mu$ l; KI, 0.5 mM; catalase, 4 units; SOD, 4 units) that were added to the SC DNA prior to the addition of the complex. For the D<sub>2</sub>O experiment, this solvent was used to dilute the sample up to 20  $\mu$ l final volume. After light exposure, each sample was incubated for 30 min at 37 °C and analyzed for the photocleaved products by gel electrophoresis.

### Conclusions

Ternary oxovanadium(IV) complexes of phenanthroline bases and curcumin or diglycosylcurcumin are presented as novel curcumin based anticancer agents. The complexes show remarkable photocytotoxicity in visible light with low dark toxicity. Coordination of curcumin or its derivative to the oxovanadium(IV) moiety significantly increases its hydrolytic stability and photocytotoxicity. This report also presents a convenient way to increase the bioavailability of curcumin dye in a metal bound form in the physiological condition. The structurally characterized complexes show DNA cleavage activity in near-IR light by generating  $\cdot$ OH radicals as the ROS. The DNA melting and viscosity data suggest intercalative mode of DNA binding of the complexes. The carbohydrate appended complexes get internalized preferentially into the cancer cells with respect to the non-carbohydrate analogue. The photocytotoxicity of **2** and **4** compares well with that of the PDT drug Photofrin<sup>®</sup>. The complexes result in apoptotic cell death by forming reactive oxygen species on photo-irradiation, while remaining as inert in dark as evidenced from the DNA laddering, annexin V-FITC/PI and DCFDA data. Confocal microscopy has

revealed mainly cytosolic localization of the complexes with significant mitochondrial uptake as observed for complex **2**. This property mimics the PDT activity of Photofrin<sup>®</sup>. In summary, incorporation of the biocompatible curcumin and its derivative and photoactive dipyrrophenazine base as the photosensitizers to an oxovanadium(IV) moiety has resulted in a significant enhancement in the stability thus bioavailability of the curcumin dye in physiological conditions and the complexes showing remarkable *in vitro* photocytotoxicity on cancer cells in visible light with low dark toxicity could open up a new vistas in the PDT chemistry.

### Acknowledgments

We thank the Department of Science and Technology (DST, Government of India), and the Council of Scientific and Industrial Research, New Delhi, for financial support (SR/S5/MBD-02/2007 and CSIR/01(2559)/12/EMR-II/2012). A.R.C. thanks the DST for J.C. Bose national fellowship. We are thankful to the Alexander von Humboldt Foundation for donation of an electrochemical system and DST for a CCD diffractometer facility. We are thankful to Sanjoy Mukherjee and Akanksha Dixit for their help in the computational and fluorescence microscopy study, respectively. S.B. thanks the University Grants Commission (UGC), New Delhi, for a research fellowship.

### Notes and references

- M. A. MacCormack, *Semin. Cutan. Med. Surg.*, 2008, **27**, 52-62.
- J. P. Celli, B. Q. Spring, I. Rizvi, C. L. Evans, K. S. Samkoe, S. Verma, B. W. Pogue and T. Hasan, *Chem. Rev.*, 2010, **110**, 2795-2838.
- A. Juzeniene, Q. Peng and J. Moan, *Photochem. Photobiol. Sci.*, 2007, **6**, 1234-1245.
- S. I. Moriwaki, J. Misawa, Y. Yoshinari, I. Yamada, M. Takigawa and Y. Tokura, *Photodermatol. Photoimmunol. Photomed.*, 2001, **17**, 241-243.
- R. Bonnett, *Chemical Aspects of Photodynamic Therapy*; Gordon & Breach: London, U.K., 2000.
- (a) H. T. Chifotides and K. R. Dunbar, *Acc. Chem. Res.*, 2005, **38**, 146-156; (b) M. A. Sgambellone, A. David, R. N. Garner, K. R. Dunbar and Claudia Turro, *J. Am. Chem. Soc.*, 2013, **135**, 11274-11282.
- (a) I. R. Canelon and P. J. Sadler, *Inorg. Chem.*, 2013, **52**, 12276-12291; (b) N. A. Smith and P. J. Sadler, *Phil. Trans. R. Soc. A.*, 2013, **371**, 20120519.
- (a) U. Schatzschneider, *Eur. J. Inorg. Chem.*, 2010, 1451-1467; (b) A. R. Chakravarty and M. Roy, *Prog. Inorg. Chem.*, 2012, **57**, 119-202.
- N. L. Fry and P. K. Mascharak, *Acc. Chem. Res.*, 2011, **44**, 289-298.
- (a) E. Wachter, D. K. Heidary, B. S. Howerton, S. Parkin and E. C. Glazer, *Chem. Commun.*, 2012, **48**, 9649-9651; (b) S. L. H. Higgins, A. J. Tucker, B. S. J. Winkel and K. J. Brewer, *Chem. Commun.*, 2012, **48**, 67-69.
- S. Banerjee, P. Prasad, A. Hussain, I. Khan, P. Kondaiah and A. R. Chakravarty, *Chem. Commun.*, 2012, **48**, 7702-7704.
- (a) H. Hatcher, R. Planalp, J. Cho, F. M. Torti and S. V. Torti, *Cell. Mol. Life Sci.*, 2008, **65**, 1631-1652; (b) V. S. Govindarajan and W. H. Stahl, *Crit. Rev. Food Sci. Nutr.*, 1980, **12**, 199-301.
- Y. P. Palve and P. L. Nayak, *Int. J. Pharm. Biomed. Sci.*, 2012, **3**, 60-69.

- A. Mukhopadhyay, C. Bueso-Ramos, D. Chatterjee, P. Pantazis and B. B. Aggarwal, *Oncogene*, 2001, **20**, 7597-7609.
- B. B. Aggarwal, C. Sundaram, N. Malani and H. Ichikawa, *Adv. Exp. Med. Biol.*, 2007, **595**, 1-75.
- P. Anand, S. G. Thomas, A. B. Kunnumakkara, C. Sundaram, K. B. Harikumar, B. Sung, S. T. Tharakan, K. Misra, I. K. Priyadarsini, K. N. Rajasekharan and B. B. Aggarwal, *Biochem. Pharmacol.*, 2008, **76**, 1590-1611.
- T. Choudhuri, S. Pal, M. L. Aggarwal, T. Das and G. Sa, *FEBS Lett.*, 2002, **512**, 334-340.
- R. Wilken, M. S. Veena, M. B. Wang and E. S. Srivatsan, *Mol. Cancer*, 2011, **10**, 1-19.
- (a) R. A. Sharma, W. P. Steward and A. J. Gescher, *Adv. Exp. Med. Biol.*, 2007, **595**, 453-470; (b) P. Anand, A. B. Kunnumakkara, R. A. Newman and B. B. Aggarwal, *Mol. Pharmaceutics*, 2007, **4**, 807-818.
- A. Hussain, K. Somyajit, B. Banik, S. Banerjee, G. Nagaraju and A. R. Chakravarty, *Dalton Trans.*, 2013, **42**, 182-195.
- S. Banerjee, P. Prasad, I. Khan, A. Hussain, P. Kondaiah and A. R. Chakravarty, *Z. Anorg. Allg. Chem.*, 2014, **640**, 1195-1204.
- (a) A. K. Renfrew, N. S. Bryce and T. W. Hambley, *Chem. Sci.*, 2013, **4**, 3731-3739; (b) D. Pucci, T. Bellini, A. Crispini, I. D'Agnano, P. F. Liguori, P. Garcia-Orduña, S. Pirillo, A. Valentini and G. Zanchettab, *Med. Chem. Commun.*, 2012, **3**, 462-468.
- F. Caruso, M. Rossi, A. Benson, C. Opazo, D. Freedman, E. Monti, M. B. Gariboldi, J. Shaulky, F. Marchetti, R. Pettinari and C. Pettinari, *J. Med. Chem.*, 2012, **55**, 1072-1081.
- S. Banerjee, A. Hussain, P. Prasad, I. Khan, B. Banik, P. Kondaiah and A. R. Chakravarty, *Eur. J. Inorg. Chem.*, 2012, 3899-3908.
- P. Prasad, I. Pant, I. Khan, P. Kondaiah and A. R. Chakravarty, *Eur. J. Inorg. Chem.*, 2014, 2420-2431.
- (a) E. Ferrari, S. Lazzari, G. Marverti, F. Pignedoli, F. Spagnolo and M. Saladini, *Biorg. Med. Chem.*, 2009, **17**, 3043-3052; (b) K. Mohri, Y. Watanabe, Y. Yoshida, M. Satoh, K. Isobe, N. Sugimoto and Y. Tsuda, *Chem. Pharm. Bull.*, 2003, **51**, 1268-1272.
- (a) M. L. Macheda, S. Rogers and J. D. Best, *J. Cell. Physiol.*, 2005, **202**, 654-662; (b) N. J. Maciver, S. R. Jacobs, H. L. Wieman, J. A. Wofford, J. L. Colloff and J. C. Rathmell, *J. Leukocyte Biol.*, 2008, **84**, 949-957.
- M. Hanif, S. M. Meier, W. Kandioller, A. Bytzeck, M. Hejl, C. G. Hartinger, A. A. Nazarov, V. B. Arion, M. A. Jakupec, P. J. Dyson and B. K. Keppler, *J. Inorg. Biochem.*, 2011, **105**, 224-231.
- I. Berger, M. Hanif, A. A. Nazarov, C. G. Hartinger, R. O. John, M. L. Kuznetsov, M. Groessl, F. Schmitt, O. Zava, F. Biba, V. B. Arion, M. Galanski, M. A. Jakupec, L. Juillerat-Jeanneret, P. J. Dyson and B. K. Keppler, *Chem. Eur. J.*, 2008, **14**, 9046-9057.
- U. Basu, I. Khan, A. Hussain, B. Gole, P. Kondaiah and A. R. Chakravarty, *Inorg. Chem.*, 2014, **53**, 2152-2162.
- (a) W. J. Geary, *Coord. Chem. Rev.*, 1971, **7**, 81-122; (b) I. Ali, W. A. Wani and K. Saleem, *Synthesis and Reactivity in Inorganic, Metal-Organic, and Nano-Metal Chemistry*, 2013, **43**, 1162-1170.
- K. Nakamoto, *Infrared and Raman Spectra of Inorganic and Coordination Compounds*, John Wiley & Sons, New York, 1997.
- (a) I. K. Priyadarsini, *J. Photochem. Photobiol. C: Photochem. Rev.*, 2009, **10**, 81-95; (b) T. A. Dahl, P. Bilski, K. J. Reszka and C. F. Chignell, *Photochem. Photobiol.*, 1994, **59**, 290-294.
- K. Tushima, R. Takano, T. Ozawa and S. Matsumura, *Chem. Commun.*, 2002, 212-213.
- P. Prasad, I. Khan, P. Kondaiah and A. R. Chakravarty, *Chem. Eur. J.*, 2013, **19**, 17445-17455.
- (a) A. D. Becke, *Phys. Rev.*, 1998, **A38**, 3098-3100; (b) A. D. Becke, *J. Chem. Phys.*, 1993, **98**, 5648-5652; (c) C. Lee, W.

- Yang and R. G. Parr, *Phys. Rev. B*, 1988, **37**, 785–789; (d) P. J. Hay and W. R. Wadt, *J. Chem. Phys.*, 1985, **82**, 284–298.
- 37 Gaussian 09, Revision A.02, M. J. Frisch, G. W. Trucks, H. B. Schlegel, G. E. Scuseria, M. A. Robb, J. R. Cheeseman, G. Scalmani, V. Barone, B. Mennucci, G. A. Petersson, H. Nakatsuji, M. Caricato, X. Li, H. P. Hratchian, A. F. Izmaylov, J. Bloino, G. Zheng, J. L. Sonnenberg, M. Hada, M. Ehara, K. Toyota, R. Fukuda, J. Hasegawa, M. Ishida, T. Nakajima, Y. Honda, O. Kitao, H. Nakai, T. Vreven, J. A. Montgomery, Jr., J. E. Peralta, F. Ogliaro, M. Bearpark, J. J. Heyd, E. Brothers, K. N. Kudin, V. N. Staroverov, R. Kobayashi, J. Normand, K. Raghavachari, A. Rendell, J. C. Burant, S. S. Iyengar, J. Tomasi, M. Cossi, N. Rega, J. M. Millam, M. Klene, J. E. Knox, J. B. Cross, V. Bakken, C. Adamo, J. Jaramillo, R. Gomperts, R. E. Stratmann, O. Yazyev, A. J. Austin, R. Cammi, C. Pomelli, J. W. Ochterski, R. L. Martin, K. Morokuma, V. G. Zakrzewski, G. A. Voth, P. Salvador, J. J. Dannenberg, S. Dapprich, A. D. Daniels, O. Farkas, J. B. Foresman, J. V. Ortiz, J. Cioslowski and D. J. Fox, Gaussian, Inc., Wallingford CT, 2009.
- 38 S. Hirohara, M. Obata, S. Ogata, K. Kajiwara, C. Ohtsuki, M. Tanihara and S. Yano, *J. Photochem. Photobiol. B: Biol.*, 2006, **84**, 56–63.
- 39 T. Mosmann, *J. Immunol. Methods*, 1983, **65**, 55–63
- 40 S. Saha, D. Mallick, R. Majumdar, M. Roy, R. R. Dighe, E. D. Jemmis and A. R. Chakravarty, *Inorg. Chem.*, 2011, **50**, 2975–2987.
- 41 E. Delaey, F. V. Laar, D. D. Vos, A. Kamuhabwa, P. Jacobs and P. D. Witte, *J. Photochem. Photobiol. B*, 2000, **55**, 27–36.
- 42 A. S. Keston and R. Brandt, *Anal. Biochem.*, 1965, **11**, 1–5.
- 43 T. Takanashi, Y. Ogura, H. Taguchi, M. Hashizoe and Y. Honda, *Invest. Ophthalmol. Vis. Sci.*, 1997, **38**, 2721–2728.
- 44 R. J. Singh, H. Karoui, M. R. Gunther, J. S. Beckman, R. P. Manson and B. Kalyanaraman, *Proc. Natl. Acad. Sci. USA*, 1998, **95**, 6675–6680.
- 45 M. Cory, D. Mckee, J. Kagan, D. Henry and J. Miller, *J. Am. Chem. Soc.*, 1985, **107**, 2528–2536.
- 46 (a) S. Tobita, M. Arakawa and I. Tanaka, *J. Phys. Chem.*, 1984, **88**, 2697–2702; (b) S. Tobita, M. Arakawa and I. Tanaka, *J. Phys. Chem.*, 1985, **89**, 5649–5654.
- 47 T. Phillips, I. Haq, A. J. H. M. Meijer, H. Adams, I. Soutar, L. Swanson, M. J. Sykes and J. A. Thomas, *Biochemistry*, 2004, **43**, 13657–13665.
- 48 (a) M. S. Vandiver, E. P. Bridges, R. L. Koon, A. N. Kinnaird, J. W. Glaeser, J. F. Campbell, C. J. Priedemann, W. T. Rosenblatt, B. J. Herbert, S. K. Wheeler, J. F. Wheeler and N. A. P. Kane-Maguire, *Inorg. Chem.*, 2010, **49**, 839–848; (b) M. Wanunu and Y. Tor, *Methods for Studying Nucleic Acid/Drug Interactions*, CRC Press, Taylor and Francis Group, 2012.
- 49 (a) B. W. Henderson, T. M. Busch, L. A. Vaughan, N. P. Frawley, D. Babich, T. A. Sosa, J. D. Zollo, A. S. Dee, M. T. Cooper, D. A. Bellnier, W. R. Greco and A. R. Oseroff, *Cancer Res.*, 2000, **60**, 525–529; (b) M. R. Detty, S. L. Gibson and S. J. Wagner, *J. Med. Chem.*, 2004, **47**, 3897–3915.
- 50 K. Szacilowski, W. Macyk, A. Drzewiecka-Matuszek, M. Brindell and G. Stochel, *Chem. Rev.*, 2005, **105**, 2647–2694.
- 51 S. E. Wolkenberg and D. L. Boger, *Chem. Rev.*, 2002, **102**, 2477–2496.
- 52 S. Xu, S. Zhang, S. Chen, M. Zhang and T. Shen, *Photochem. Photobiol. Sci.*, 2003, **2**, 871–876.
- 53 O. Vajragupta, P. Boonchoong and L. Berliner, *Free Radic. Res.*, 2004, **38**, 303–314.
- 54 D. D. Perrin, W. L. F. Armarego and D. R. Perrin, *Purification of Laboratory Chemicals*; Pergamon Press: Oxford, 1980.
- 55 (a) J. G. Collins, A. D. Sleeman, J. R. Aldrich-Wright, I. Greguric and T. W. Hambley, *Inorg. Chem.*, 1998, **37**, 3133–3141; (b) E. Amouyal, A. Homsy, J.-C. Chambron and J.-P. Sauvage, *J. Chem. Soc. Dalton Trans.*, 1990, 1841–1845.
- 56 J. Guilford II, R. Jackson, C. Choi and W. R. Bergmark, *J. Phys. Chem.*, 1985, **89**, 294–300.
- 57 J. R. Lakowicz, *Principles of Fluorescence Spectroscopy*, Kluwer Academic/Plenum Publishers, New York, 1999.
- 58 A. T. R. Williams, S. A. Winfield and J. N. Miller, *Analyst*, 1983, **108**, 1067–1071.
- 59 N. Walker and D. Stuart, *Acta Crystallogr.*, 1983, **A39**, 158–166.
- 60 G. M. Sheldrick, *SHELX-97, Programs for Crystal Structure Solution and Refinement*; University of Göttingen, Göttingen, Germany, 1997.
- 61 J. L. Farrugia, *J. Appl. Crystallogr.*, 1999, **32**, 837–838.
- 62 A. L. Spek, PLATON. A Multipurpose Crystallographic Tool, Utrecht University, the Netherlands, 2002.
- 63 H.J. Motulsky, Prism 5 Statistics Guide, 2007, GraphPad Software Inc., San Diego CA, www.graphpad.com.
- 64 D.-R. Xu, S. Hung, Z.-J. Long, J.-J. Chen, Z.-Z. Zou, J. Li, D.-J. Lin and Q. Liu, *J. Transl. Med.*, 2011, **9**, 74.
- 65 K. Million, É. Horvilleur, D. Goldschneider, M. Agina, G. Raguénez, F. Tournier, J. Bénard and S. Douc-Rasy, *Int. J. Oncol.*, 2006, **29**, 147–154.
- 66 J. D. McGhee and P. H. von Hippel, *J. Mol. Biol.*, 1974, **86**, 469–489.
- 67 M. T. Carter, M. Rodriguez and A. J. Bard, *J. Am. Chem. Soc.*, 1989, **111**, 8901–8911.
- 68 J. Bernadou, G. Pratiel, F. Bennis, M. Girardet and B. Meunier, *Biochemistry*, 1989, **28**, 7268–7275.

**Table 2.** Selected bond distances (Å) and angles (°) for [VO(cur)(phen)Cl] (1) with e.s.d.s in the parentheses

V(1)–N(1)	2.128(5)	N(2)–V(1)–O(3)	163.4(2)
V(1)–N(2)	2.116(5)	N(2)–V(1)–O(4)	92.28(17)
V(1)–O(3)	1.973(5)	N(2)–V(1)–O(7)	95.0(2)
V(1)–O(4)	1.959(4)	N(2)–V(1)–Cl(1)	80.71(14)
V(1)–O(7)	1.536(5)	O(3)–V(1)–O(4)	90.46(17)
V(1)–Cl(1)	2.783(2)	O(3)–V(1)–O(7)	100.4(2)
N(1)–V(1)–N(2)	78.12(18)	O(3)–V(1)–Cl(1)	83.53(15)
N(1)–V(1)–O(3)	94.10(18)	O(4)–V(1)–O(7)	101.96(19)
N(1)–V(1)–O(4)	160.3(2)	O(4)–V(1)–Cl(1)	81.47(14)
N(1)–V(1)–O(7)	96.1(2)	O(7)–V(1)–Cl(1)	174.65(14)
N(1)–V(1)–Cl(1)	79.98(15)		

75

**Table 1.** Selected physicochemical data and ct-DNA binding parameters of the complexes **1** - **4**

Complex	IR <sup>a</sup> / cm <sup>-1</sup>		$\lambda_{\max}$ / nm ( $\epsilon/\text{dm}^3 \text{ mol}^{-1}$ cm <sup>-1</sup> ) <sup>b</sup>	$\lambda_f$ / nm [ $\Phi_f$ ] <sup>c</sup>	$\mu_{\text{eff}}$ <sup>d</sup>	$\Lambda_M$ <sup>e</sup>	$E_{\text{pc}}$ <sup>f</sup> / V	$K_b$ <sup>g</sup> / mol <sup>-1</sup>	$\Delta T_m$ <sup>h</sup> / °C
	$\tilde{\nu}$ (C=O)	$\tilde{\nu}$ (V=O)							
<b>1</b>	1590	966	721 (54)	515 [0.008]	1.67	104	-1.29	(6.1±0.4) x 10 <sup>4</sup>	2.0
<b>2</b>	1587	968	731 (64)	518 [0.01]	1.61	96	-1.22	(5.6±0.5) x 10 <sup>5</sup>	5.4
<b>3</b>	1585	964	752 (55)	506 [0.01]	1.69	90	-1.34	(8.4±0.3) x 10 <sup>4</sup>	4.2
<b>4</b>	1588	961	749 (67)	509 [0.015]	1.64	87	-1.15	(7.2±0.2) x 10 <sup>5</sup>	6.9

<sup>a</sup> In solid phase. <sup>b</sup> In 10% DMF-water. <sup>c</sup> In 10% aqueous DMSO. <sup>d</sup>  $\mu_{\text{eff}}$  in  $\mu_B$  using DMSO-*d*<sub>6</sub> solutions of the oxovanadium(IV) complexes at 25 °C. <sup>e</sup>  $\Lambda_M$ , molar conductivity in S cm<sup>2</sup> mol<sup>-1</sup> in 10% aqueous DMF at 25 °C. The complexes are non-electrolytic in pure DMF. <sup>f</sup> In 20% DMF-H<sub>2</sub>O with 0.1M TBAP. The potentials are vs. SCE at a scan rate of 50 mV s<sup>-1</sup>.  $E_{\text{pc}}$  is the cathodic peak potential. <sup>g</sup> Intrinsic ct-DNA binding constant ( $K_b$ ). <sup>h</sup> Change in the calf thymus DNA melting temperature.

100

**Table 3:** IC<sub>50</sub> (μM) values of different curcumin complexes and other relevant compounds in different cells

Compound	HeLa		HaCaT		MCF-7	
	(Light) <sup>a</sup>	(Dark) <sup>b</sup>	(Light) <sup>a</sup>	(Dark) <sup>b</sup>	(Light) <sup>a</sup>	(Dark) <sup>b</sup>
<b>1</b>	8.1±0.3	>50	6.4±0.3	46±1	10±1	>50
<b>2</b>	3.3±0.4	>50	2.3±0.2	43±1	4.7±0.3	>50
<b>3</b>	4.6±0.2	46±1	3.5±0.2	40±2	5.8±0.2	>50
<b>4</b>	1.5±0.2	45±1	0.63±0.02	34±1	2.4±0.1	>50
Curcumin (Hcur)	8.2±0.2	85±4	19±1	28±1	20±2	90±5
Hscur	>50	>50	>50	>50	>50	>50
[La(py-tpy)(cur)(NO <sub>3</sub> ) <sub>2</sub> ] <sup>c</sup>	4.6±0.6	>100				
[(p-cymene)Ru(cur)Cl] <sup>d</sup>						19.58 ± 2.37 <sup>e</sup>
Cisplatin <sup>f</sup>	68.7±3.4	71.3±2.9				

<sup>a</sup> For 4 h incubation in the dark followed by exposure to visible light of 400-700 nm (10 J cm<sup>-2</sup>) for 1h. <sup>b</sup> For 4 h incubation in the dark. <sup>c</sup> Data from ref. 20. <sup>d</sup> From ref. 23. <sup>e</sup> 72 h incubation in dark. <sup>f</sup> From ref. 40 for an incubation time of 4 h.

**Table 4.** Selected SC pUC19 DNA (0.2 μg) cleavage data of the complexes **1-4** and the ligands in red light

Reaction condition <sup>a</sup>	% NC Form	% NC Form	% NC Form
	(In dark)	(Red light, 705 nm)	(Red light, 785 nm)
DNA control	2	3	4
DNA + <b>1</b>	5	42	38
DNA + <b>2</b>	10	90	87
DNA + <b>3</b>	4	46	45
DNA + <b>4</b>	8	92	94
DNA + curcumin (Hcur)	11	15	16
DNA + Hscur	13	18	18

<sup>a</sup> In Tris-buffer medium (pH =7.2). Red light from diode lasers. Photo-exposure time (t) = 1 h. Concentration of the complexes (**1-4**) and the ligands was 40 μM.

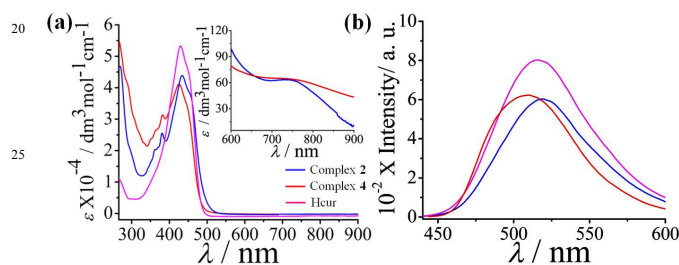
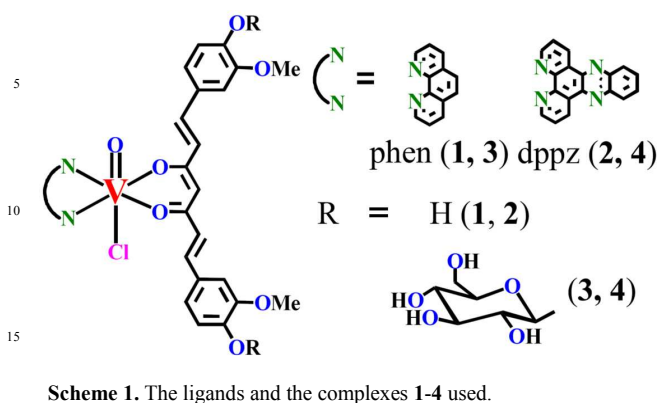


**Fig. 1** (a) Absorption spectra of curcumin (Hcur) ligand and the complexes 2 and 4 in 10% aqueous DMF. The inset shows the d-d band of the oxovanadium(IV) complexes. (b) Fluorescence spectra of Hcur and the complexes 2 and 4 in 10% aqueous DMSO ( $\lambda_{ex} = 420$  nm).

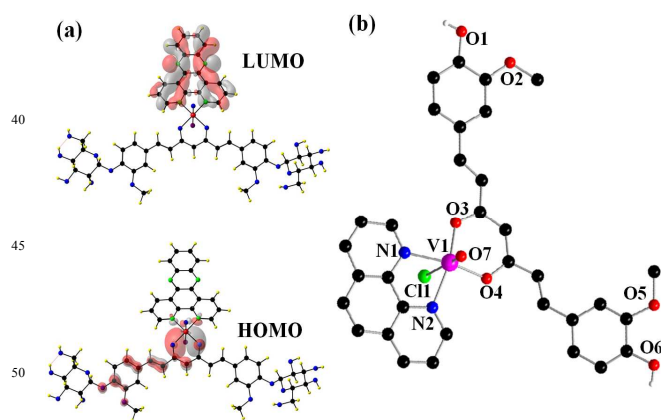


**Fig. 2** (a) HOMO-LUMO of complex 4 using energy optimized structure. (b) Reproduced crystal structure of complex 1.<sup>11</sup>

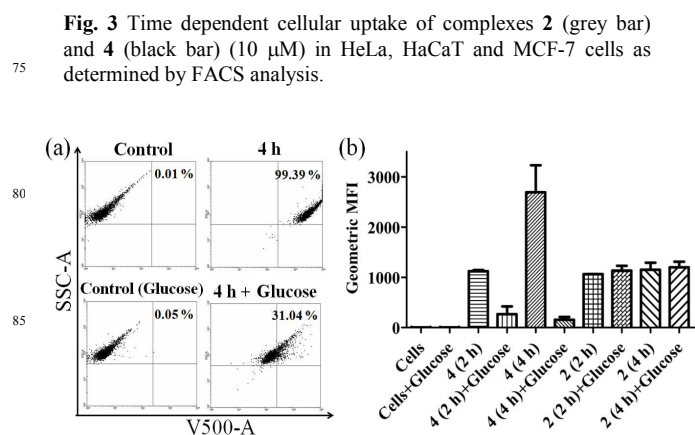
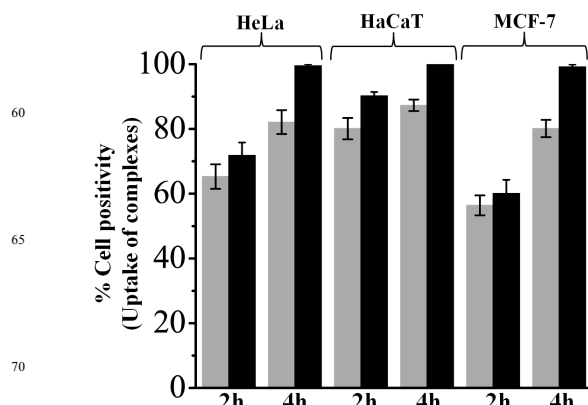


**Fig. 4** (a) Comparison of the (a) cellular uptake of complex 4 (10  $\mu$ M) at 4 h of incubation with HeLa cells in absence of excess added sugar and after pre-incubation with higher glucose concentration (10 mM) as determined from the FACS analysis. (b) Mean fluorescence intensity (MFI) demonstrating the mean complex uptake in cells for 2 and 4 under above mentioned condition.

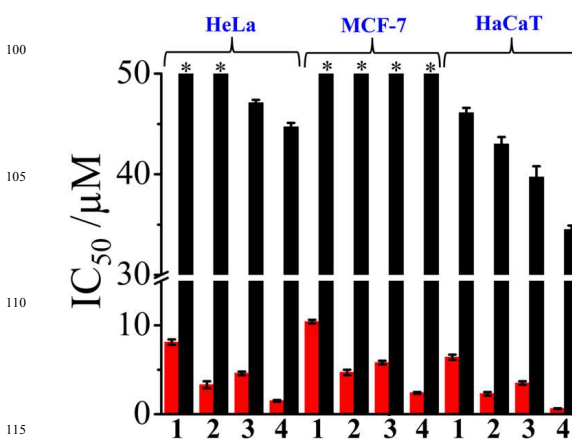


**Fig. 5** Photocytotoxicity of the complexes 1-4 in HeLa, MCF-7 and HaCaT cells on 4 h incubation in dark (black bar) followed by photo-irradiation with visible light of 400–700 nm (10  $J$   $cm^{-2}$ ) (red bar). Samples tested up to 50  $\mu$ M concentration are marked as \*.

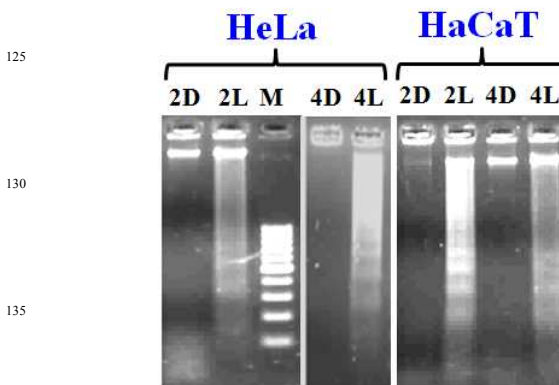


**Fig. 6** DNA ladder of complexes 2 and 4 showing apoptosis in HeLa and HaCaT cells caused on photo-exposure to visible light (400–700 nm): D, in dark; L, in light and M, 100 b.p. DNA ladder.

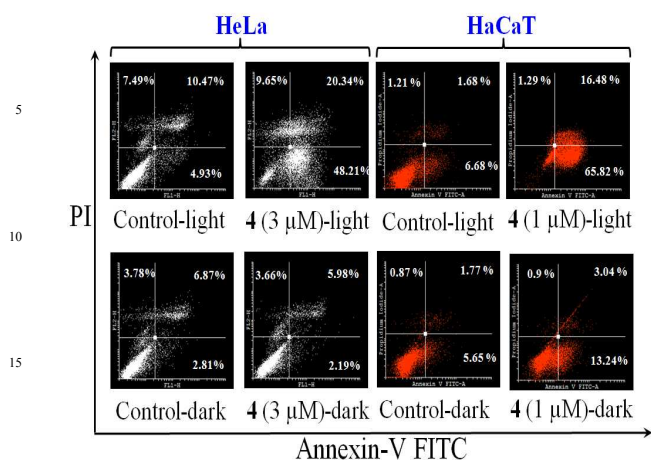


**Fig. 7** FACS profiles of Annexin-V FITC and PI staining of HeLa and HaCaT cells undergoing early apoptosis induced by complex 4 in visible light (400-700 nm) while remaining nontoxic in dark.

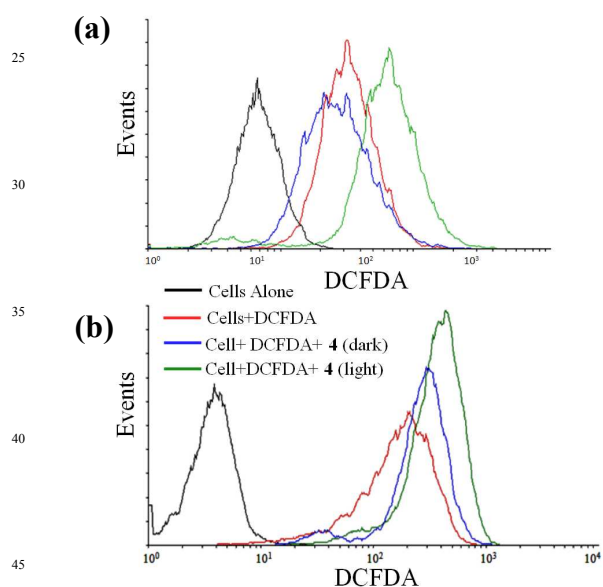


**Fig. 8** Flow cytometric analysis (FACS) for ROS generation by complex 4 was performed using DCFDA dye. Generation of ROS is highlighted by the shift in fluorescence band positions compared to cells alone in (a) HeLa and (b) HaCaT cells treated with complex 4, under different experimental conditions as shown by the color codes. Greater shift implies higher amount of DCF and thus greater ROS generation.

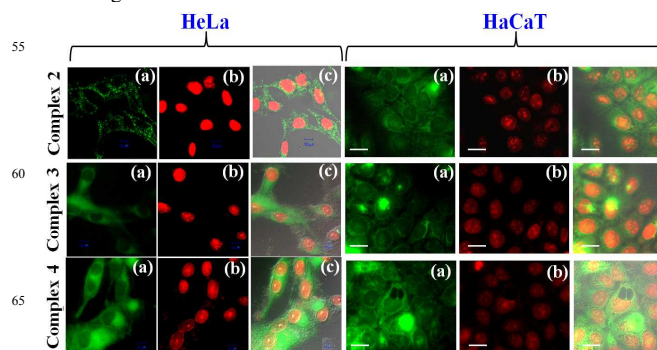


**Fig. 9** Confocal images of HeLa and HaCaT cells (after 4 h) treated with complexes 2-4 (10  $\mu$ M) and propidium iodide (PI, 1 mg ml<sup>-1</sup>): Panels: (a) fluorescence of the complex, (b) fluorescence of PI and (c) merged image of (a) and (b). Scale bar = 10  $\mu$ m.

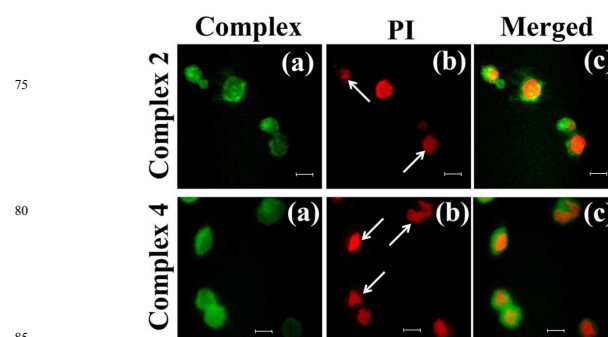


**Fig. 10** Confocal images of complexes 2 (5  $\mu$ M) and 4 (3  $\mu$ M) in HaCaT cells. Panels (a), (d), (g) and (j) show fluorescence of 2. Panels (a) are for the complex green fluorescence; Panels (b) for PI-staining. Panels (c) are the merged images. The PDT effect, visible only in light, is shown by arrows in panels (b) Scale bar: 10  $\mu$ m.

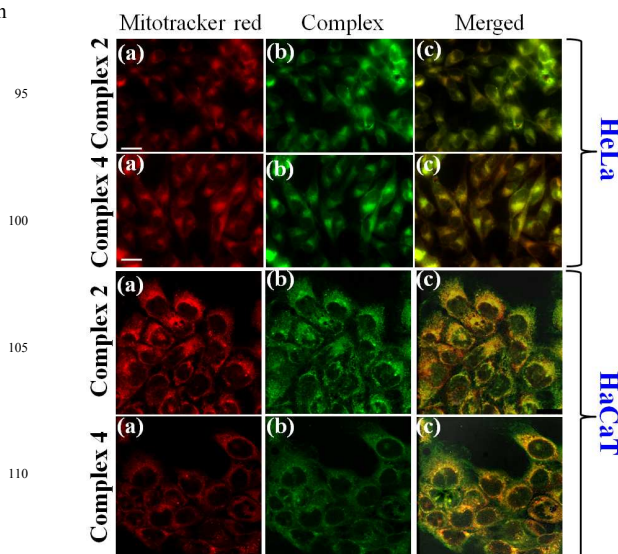


**Fig. 11** Fluorescence microscopic images of complexes 2 and 4 (10  $\mu$ M) and Mito-tracker deep red (MTR, 50 nM) in HeLa and HaCaT cells after 4 h incubation: panels (a) show fluorescence of MTR; panels (b) show fluorescence images of 2 and 4 respectively and panels (c) show the merged image of MTR and the complexes. Scale bar: 20  $\mu$ m.

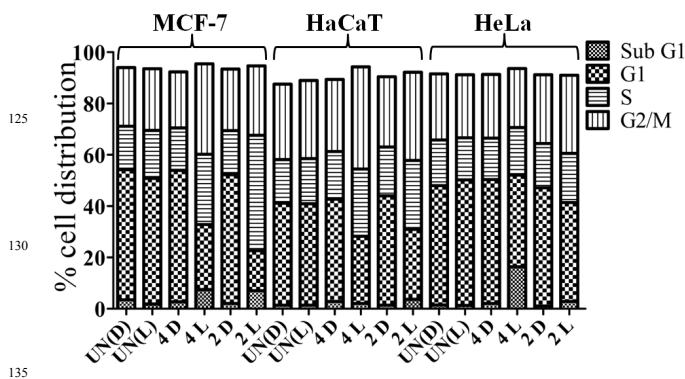


**Fig. 12** Bar diagram showing % distribution of MCF-7, HaCaT and HeLa cells treated with complex 2 (5  $\mu$ M in MCF-7, 3  $\mu$ M in HaCaT and 4  $\mu$ M in HeLa) and complex 4 (3  $\mu$ M in MCF-7, 1  $\mu$ M in HaCaT and 2  $\mu$ M in HeLa). UN(D) = untreated dark control, UN(L) = untreated light control, D = dark, L = light of 400-700 nm.

# Remarkable enhancement in photocytotoxicity and hydrolytic stability of curcumin on binding to an oxovanadium(IV) moiety †

Samya Banerjee,<sup>a</sup> Ila Pant,<sup>b</sup> Imran Khan,<sup>b</sup> Puja Prasad,<sup>a</sup> Akhtar Hussain,<sup>a</sup> Paturu Kondaiah\*,<sup>b</sup> and Akhil R. Chakravarty\*<sup>a</sup>

**Keywords :** Curcumin, Oxovanadium(IV), Apoptotic photocytotoxicity, Cellular imaging, mitochondria targeting

**Synopsis (20 words):** Polypyridyl oxovanadium(IV) curcumin complexes show remarkable hydrolytic stability and visible light-induced photocytotoxicity in cancer cells by mitochondria targeting ROS-mediated apoptosis.

## Pictogram:

